Received: 26 October 2019 | Revised: 18 December 2019 | Accepted: 15 January 2020

DOI: 10.1002/jbio.201960167

FULL ARTICLE

JOURNAL OF BIOPHOTONICS

Dual- and single-shot susceptibility ratio measurements with circular polarizations in second-harmonic generation microscopy

Ahmad Golaraei[1,2,3] | **Lukas Kontenis**[4,5] | **Abiramy Karunendiran**[6,7] | **Bryan A. Stewart**[6,7] | **Virginijus Barzda**[2,3,5*]

[1]Princess Margaret Cancer Centre, University Health Network, Toronto, Ontario, Canada

[2]Department of Physics, University of Toronto, Toronto, Ontario, Canada

[3]Department of Chemical and Physical Sciences, University of Toronto Mississauga, Mississauga, Ontario, Canada

[4]Light Conversion, Vilnius, Lithuania

[5]Faculty of Physics, Laser Research Centre, Vilnius University, Vilnius, Lithuania

[6]Department of Biology, University of Toronto Mississauga, Mississauga, Ontario, Canada

[7]Department of Cell and Systems Biology, University of Toronto, Toronto, Ontario, Canada

***Correspondence**
Virginijus Barzda, Department of Chemical and Physical Sciences, University of Toronto Mississauga, 3359 Mississauga Rd. North, Mississauga, ON L5L 1C6, Canada.
Email: virgis.barzda@utoronto.ca

Present address
Virginijus Barzda, Department of Chemical and Physical Sciences, University of Toronto Mississauga, 3359 Mississauga Rd. North, Mississauga, ON L5L 1C6

Funding information
Canadian Institutes of Health Research, Grant/Award Number: CPG-134752; European Regional Development Fund, Grant/Award Number: 01.2.2.-LMT-K-718-02-0016; Natural Sciences and Engineering Research Council of Canada, Grant/Award Numbers: CHRPJ 462842-14, DGDND-2017-00099, RGPIN-2017- 06923

Abstract

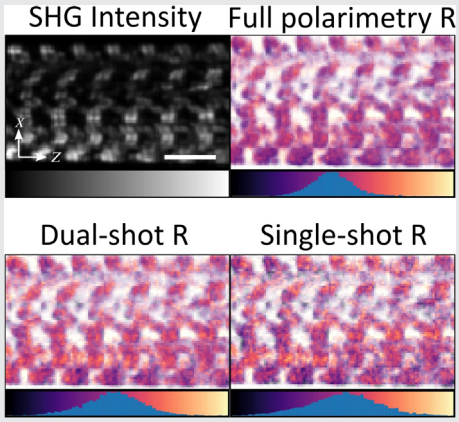

Polarization-resolved second-harmonic generation (P-SHG) microscopy is a technique capable of characterizing nonlinear optical properties of noncentrosymmetric biomaterials by extracting the nonlinear susceptibility tensor components ratio $\chi^{(2)'}_{zzz}/\chi^{(2)'}_{zxx}$, with z-axis parallel and x-axis perpendicular to the C_6 symmetry axis of molecular fiber, such as a myofibril or a collagen fiber. In this paper, we present two P-SHG techniques based on incoming and outgoing circular polarization states for a fast extraction of $\chi^{(2)'}_{zzz}/\chi^{(2)'}_{zxx}$: A dual-shot configuration where the SHG circular anisotropy generated using incident right- and left-handed circularly-polarized light is measured; and a single-shot configuration for which the SHG circular anisotropy is measured using only one incident circular polarization state. These techniques are used to extract the $\chi^{(2)'}_{zzz}/\chi^{(2)'}_{zxx}$ of myosin fibrils in the body wall muscles of *Drosophila melanogaster* larva. The results are in good agreement with values obtained from the double Stokes-

Ahmad Golaraei and Lukas Kontenis have contributed equally to this paper.

Mueller polarimetry. The dual- and single-shot circular anisotropy measurements can be used for fast imaging that is independent of the in-plane orientation of the sample. They can be used for imaging of contracting muscles, or for high throughput imaging of large sample areas.

KEYWORDS

muscle, nonlinear optical polarimetry, second-harmonic generation microscopy, second-order susceptibility

1 | INTRODUCTION

Second-harmonic generation (SHG) microscopy is a powerful technique for imaging noncentrosymmetric biomaterials such as collagen fibers [1–4], myosin filaments [5–10], microtubules [11, 12], and starch granules [13–16]. The SHG efficiency is characterized by the second-order susceptibility tensor $\chi^{(2)}$ whose elements depend on the composition and the 3D organization of the SHG-active molecules. The polarimetric SHG (P-SHG) can be used for extracting the values of $\chi^{(2)}$ tensor elements. The simplest P-SHG implementation involves rotating the plane of linear polarization of the incident beam and measuring the intensity of the SHG response of the material. This method has been used to study various biological structures [1–3, 5, 6, 17–24]. Other techniques, such as linear polarization-in, polarization-out (PIPO) SHG microscopy [25], involve changing the incident linear polarization states and measuring the linear polarization of the outgoing SHG signal from the sample, which results in a more detailed polarization response analysis. Recently, a complete SHG polarimetry technique–double Stokes-Mueller polarimetry (DSMP) [26, 27] –was developed based on a generalized Stokes-Mueller formalism. Using DSMP, 36 P-SHG measurements are sufficient to completely characterize the 2D nonlinear polarization properties of the material.

The most often used P-SHG parameter for structural characterization is the second-order susceptibility ratio $R = \chi^{(2)'}_{zzz} / \chi^{(2)'}_{zxx} \cdot \chi^{(2)'}_{zzz}$ is the susceptibility tensor element for which the generated second harmonic electric field and incident light electric field are along the C_6 symmetry axis of the molecular fiber, such as myofibril or collagen fiber (z) and $\chi^{(2)'}_{zxx}$ is the susceptibility tensor element for which the SHG electric field is along z-axis and the incident light electric field is perpendicular to it. The R-ratio has been previously used to characterize different biomaterials such as tendon [1, 19, 25, 28–31], bone [32], muscle [8, 26, 27, 33–35], and starch [15, 16]. The R-ratio was further used to differentiate between normal and cancerous tissues in various organs such as lung [36], breast [37], thyroid [38], and pancreas [39]. The R-ratio measurement can be used as a complementary method along with other histopathology techniques for tissue characterization and differentiation.

Although the R-ratio can be used as a structural biomarker, its measurement is usually accomplished by acquiring many images with different input and output polarization states, which is time-consuming and therefore technically challenging for applications where imaging of fast dynamic processes is required, or for clinical applications where low-intensity laser exposure is necessary. The acquisition time of a polarimetric dataset in SHG microscopy can be shortened by employing motorized fast polarization rotators [9], liquid crystal retarders [40], and electro-optical modulators [41–43] synchronized with the scanning mirrors. Staggered laser pulses for fast polarization switching can also be used [44, 45]. Fast polarimetric detection is usually accomplished by measuring several polarization states in parallel on separate detectors [10, 41, 46, 47]. For example, a single-shot (scan) orientation-independent polarimetric measurement of the R-ratio was accomplished with circularly polarized incident light and three parallel detectors acquiring different linear SHG polarizations [10]. In addition, using only one detector and four linear incoming polarization states an estimation of the R-ratio as well as the orientation of the fibers in the sample were deduced [48].

In this paper, we utilize incident and outgoing circular polarizations for the R-ratio imaging, and ultimately use only two outgoing orthogonal polarization states which provide the minimum number of measurements to determine the R-ratio. Since we only use incoming and outgoing circular polarizations, this technique is independent of the sample orientation in the image plane. Dual- and single-shot measurement techniques are presented in this paper. The dual-shot technique involves measuring circular anisotropy of the SHG signal produced using right- and left-hand circularly polarized incident light (RCP and LCP, respectively), and therefore, it is called a circular anisotropy of circular dichroism (CA_{CD}). The CA_{CD} expression and its relation to the R-ratio is derived from the DSMP formalism [26]. The measurement of the R-ratio using the CA_{CD} parameter is verified by

comparing it to the *R*-ratio obtained from a full DSMP measurement. If the chiral susceptibility contribution is negligible, the *R*-ratio measurements can be further simplified to a circular anisotropy measurement with only one incident circular polarization state, providing a single-shot estimation of the *R*-ratio. The *R*-ratios extracted with incident RCP and LCP states are also compared to *R*-ratios from DSMP measurements as well as the dual-shot CA_{CD} technique. The *R*-ratio measurement techniques are demonstrated for muscle tissue, which is a commonly studied biological sample in P-SHG microscopy.

The dual-shot measurement (with two measurements of the orthogonal outgoing circular polarization states) and single-shot measurement (with only one parallel measurement of two orthogonal states) are much faster than full DSMP (with 36 measurements) or PIPO (with 81 measurements) techniques. Therefore, dual- and single-shot polarimetry measurements using circular polarizations enable new applications of P-SHG microscopy for the imaging of fast kinetic processes such as the flickering of sarcomeres during muscle contraction [49], and also in large-area polarimetric tissue imaging where high imaging throughput is essential. In this paper, we validate the dual- and single-shot polarimetry experiments using the full DSMP data set.

2 | THEORETICAL BACKGROUNDS

Nonlinear optical properties of the material responsible for SHG can be succinctly described using double Stokes-Mueller polarimetry (DSMP) formalism [26]. In a DSMP measurement, the incident laser beam is described by a nine element ($N = 0...9$) double Stokes vector. The incident beam is switched over a set of nine input polarization states ($Q = 1...9$), S_Q: horizontally (0° or HLP), vertically (90° or VLP), and diagonally linearly polarized ($\pm 45^\circ$), right-hand and left-hand circularly polarized (RCP and LCP, respectively), linearly polarized at -22.5°, and right- and left-hand elliptically polarized (REP and LEP, respectively). The double Stokes vector elements for this set are given in Samim et al [26]. The incoming polarization set $S_{N,Q}$ represents an invertible double Stokes matrix. For every incident polarization state, a conventional 4×1 Stokes vector s'_γ with $\gamma = 0...3$ of the outgoing SHG signal is measured. The resulting 4×9 Stokes measurement matrix $s'_{\gamma,Q}$ then contains 36 values:

$$s'_{\gamma,Q} = \mathcal{M}^{(2)}_{\gamma,N} S_{N,Q}, \tag{1}$$

where Einstein summation is assumed over the index *N*. The $\mathcal{M}^{(2)}$ matrix can be obtained by inverting the $S_{N,Q}$ matrix [26]. The $\mathcal{M}^{(2)}$ matrix is a function of the second-order susceptibilities and it fully characterizes the 2D second-order polarization properties of the sample. Even though as little as 36 measurements are required to fully characterize the sample in SHG, in many cases even fewer measurements are sufficient to retrieve the *R*-ratio via various reduced polarimetry methods. We will present two fast measurement techniques, which only use circularly polarized incident and outgoing light to extract the *R*-ratio. Circular anisotropy of the circular dichroism, (CA_{CD}), can be defined as the difference in the s_3 Stokes components of the outgoing SHG when generated by RCP (for which $Q = 5$) and LCP (for which $Q = 6$) incident light. It can be formulated as follows:

$$CA_{CD} = 2\frac{s'_{3,5} - s'_{3,6}}{s'_{0,5} + s'_{0,6}}. \tag{2}$$

Using Equation (2), and the definition of $S_{N,Q}$ for an SHG process [26], CA_{CD} can be rewritten as a function of the Mueller matrix elements:

$$CA_{CD} = 4\frac{\mathcal{M}_{3,8} - \mathcal{M}_{3,9}}{\sqrt{6}\mathcal{M}_{0,1} - \sqrt{3}\mathcal{M}_{0,2} - \mathcal{M}_{0,4}}. \tag{3}$$

The Mueller matrix elements are functions of the $\chi^{(2)}$ tensor elements in the laboratory coordinate system and their associated phase differences [26]:

$$\mathcal{M}_{0,1} = \frac{\sqrt{6}}{6}\left(\left(\left|\chi^{(2)}_{ZXX}\right|^2 + \left|\chi^{(2)}_{ZZZ}\right|^2 + \left|\chi^{(2)}_{ZXZ}\right|^2\right) + \left(\left|\chi^{(2)}_{XXX}\right|^2 + \left|\chi^{(2)}_{XZZ}\right|^2 + \left|\chi^{(2)}_{XXZ}\right|^2\right)\right), \tag{4a}$$

$$\mathcal{M}_{0,2} = \frac{\sqrt{3}}{6}\left(\left(\left|\chi^{(2)}_{ZXX}\right|^2 + \left|\chi^{(2)}_{ZZZ}\right|^2 - 2\left|\chi^{(2)}_{ZXZ}\right|^2\right) + \left(\left|\chi^{(2)}_{XXX}\right|^2 + \left|\chi^{(2)}_{XZZ}\right|^2 - 2\left|\chi^{(2)}_{XXZ}\right|^2\right)\right), \tag{4b}$$

$$\mathcal{M}_{0,4} = \left|\chi^{(2)}_{ZZZ}\right|\left|\chi^{(2)}_{ZXX}\right|\cos\Delta_{ZZZ,ZXX} + \left|\chi^{(2)}_{XXX}\right|\left|\chi^{(2)}_{XZZ}\right|\cos\Delta_{XXX,XZZ}, \tag{4c}$$

$$\mathcal{M}_{3,8} = \left|\chi^{(2)}_{ZZZ}\right|\left|\chi^{(2)}_{XXZ}\right|\cos\Delta_{ZZZ,XXZ} - \left|\chi^{(2)}_{XZZ}\right|\left|\chi^{(2)}_{ZXZ}\right|\cos\Delta_{XZZ,ZXZ}, \tag{4d}$$

$$\mathcal{M}_{3,9} = \left|\chi^{(2)}_{ZXX}\right|\left|\chi^{(2)}_{XXZ}\right|\cos\Delta_{ZXX,XXZ} + \left|\chi^{(2)}_{XXX}\right|\left|\chi^{(2)}_{ZXZ}\right|\cos\Delta_{XXX,ZXZ}, \tag{4e}$$

where *XYZ* indices correspond to the Cartesian laboratory coordinate system. In this coordinate system, the sample is placed in the *XZ*-plane and the laser beam propagates along the *Y*-axis.

In general, $\chi^{(2)}$ is a complex number and it can be defined as $\chi^{(2)}_{IJK} = \left|\chi^{(2)}_{IJK}\right| e^{i\xi_{IJK}}$. Therefore, $\Delta_{IJK,I'J'K'} = \xi_{IJK} - \xi_{I'J'K'}$ is the phase difference between $\chi^{(2)}_{IJK}$ and $\chi^{(2)}_{I'J'K'}$. In addition, the sample is generally rotated with respect to the laboratory-frame, and therefore, the $\chi^{(2)}_{IJK}$ elements are related to the intrinsic molecular second-order susceptibility tensor elements $\chi^{(2)}_{ijk}$, via a rotation matrix [29]. In an SHG process, $\chi^{(2)}_{ijk}$ has 18 independent elements. For specific symmetry classes, however, the number of independent elements can be reduced. Since many biological structures, such as myosin, are helical, they can be described by a C_6 symmetry class which reduces the number of nonzero independent $\chi^{(2)}_{ijk}$ elements to four: $\chi^{(2)}_{zzz}, \chi^{(2)}_{zxx}, \chi^{(2)}_{xxz}, \chi^{(2)}_{xyz}$. For the case of C_6 symmetry, the $\chi^{(2)}_{IJK}$ elements can be written in terms of the molecular $\chi^{(2)}_{ijk}$ elements and the 3D orientation angles of the sample as follows [29]:

$$\chi^{(2)}_{XXX} = \cos\alpha\sin\delta\left[\left(\chi^{(2)}_{zzz} - 2\chi^{(2)}_{xxz} - \chi^{(2)}_{zxx}\right)\cos^2\alpha\sin^2\delta + 2\chi^{(2)}_{xxz} + \chi^{(2)}_{zxx}\right], \tag{5a}$$

$$\chi^{(2)}_{XXZ} = \cos\alpha\cos\delta\left[\left(\chi^{(2)}_{zzz} - 2\chi^{(2)}_{xxz} - \chi^{(2)}_{zxx}\right)\cos^2\alpha\sin^2\delta + \chi^{(2)}_{xxz}\right] - \frac{1}{2}\chi^{(2)}_{xyz}\sin(2\alpha)\sin\delta, \tag{5b}$$

$$\chi^{(2)}_{XZZ} = \cos\alpha\sin\delta\left[\left(\chi^{(2)}_{zzz} - 2\chi^{(2)}_{xxz} - \chi^{(2)}_{zxx}\right)\cos^2\alpha\cos^2\delta + \chi^{(2)}_{zxx}\right] - \chi^{(2)}_{xyz}\sin 2\alpha\cos\delta, \tag{5c}$$

$$\chi^{(2)}_{ZXX} = \cos\alpha\cos\delta\left[\left(\chi^{(2)}_{zzz} - 2\chi^{(2)}_{xxz} - \chi^{(2)}_{zxx}\right)\cos^2\alpha\sin^2\delta + \chi^{(2)}_{zxx}\right] + \chi^{(2)}_{xyz}\sin(2\alpha)\sin\delta, \tag{5d}$$

$$\chi^{(2)}_{ZXZ} = \cos\alpha\sin\delta\left[\left(\chi^{(2)}_{zzz} - 2\chi^{(2)}_{xxz} - \chi^{(2)}_{zxx}\right)\cos^2\alpha\cos^2\delta + \chi^{(2)}_{xxz}\right] + \frac{1}{2}\chi^{(2)}_{xyz}\sin(2\alpha)\cos\delta, \tag{5e}$$

$$\chi^{(2)}_{ZZZ} = \cos\alpha\cos\delta\left[\left(\chi^{(2)}_{zzz} - 2\chi^{(2)}_{xxz} - \chi^{(2)}_{zxx}\right)\cos^2\alpha\cos^2\delta + 2\chi^{(2)}_{xxz} + \chi^{(2)}_{zxx}\right], \tag{5f}$$

where α is the out-of-plane tilt angle with respect to the *XZ* image plane, and δ is the average in-plane fiber orientation angle measured from the *Z*-axis in the laboratory frame of reference. By substituting Equations (4) and (5) in Equation (3), the CA_{CD} can be obtained in terms of the products of the magnitudes of the molecular susceptibility tensor elements, $\left|\chi^{(2)}_{ijk}\right|\left|\chi^{(2)}_{i'j'k'}\right|$, the associated molecular phase differences, $\Delta_{ijk,i'j'k'} = \zeta_{ijk} - \zeta_{i'j'k'}$, and the out-of-plane tilt angle of the collagen fibers, α. The numerator of Equation (3) can be expressed as:

$$\begin{aligned} CA_{CD,numerator} &= 4\left|\chi^{(2)}_{xxz}\right|\cos^2(\alpha)\left[\left|\chi^{(2)}_{zzz}\right|\cos^2(\alpha)\cos\Delta_{zzz,xxz}\right. \\ &- \left|\chi^{(2)}_{zxx}\right|\cos^2(\alpha)\cos\Delta_{zxx,xxz} \\ &\left. + 2\left|\chi^{(2)}_{xxz}\right|\sin^2(\alpha)\right] + 2\left|\chi^{(2)}_{xyz}\right|^2\sin^2(2\alpha), \end{aligned} \tag{6}$$

and the denominator can be expressed as:

$$\begin{aligned} CA_{CD,denominator} &= 0.5\left|\chi^{(2)}_{zzz}\right|^2\cos^6(\alpha) + 0.5\left|\chi^{(2)}_{zxx}\right|^2\cos^6(\alpha) \\ &+ 2\left|\chi^{(2)}_{xxz}\right|^2\left(\cos^6\alpha - 2\cos^4\alpha + 2\cos^2\alpha\right) \\ &- \left|\chi^{(2)}_{zzz}\right|\left|\chi^{(2)}_{zxx}\right|\cos\Delta_{zzz,zxx}\cos^6\alpha \\ &+ 2\left|\chi^{(2)}_{zzz}\right|\left|\chi^{(2)}_{xxz}\right|\cos\Delta_{zzz,xxz}\left(\cos^4\alpha - \cos^6\alpha\right) \\ &+ 2\left|\chi^{(2)}_{zxx}\right|\left|\chi^{(2)}_{xxz}\right|\cos\Delta_{zxx,xxz}\left(\cos^6\alpha - \cos^4\alpha\right) \\ &+ \left|\chi^{(2)}_{xyz}\right|^2\sin^2 2\alpha. \end{aligned} \tag{7}$$

The in-plane fiber angle, δ, is absent from the Equations (6) and (7) indicating that, for incoming circular polarization, CA_{CD} is independent of the orientation of the sample in the image plane. Equations (6) and (7) show that CA_{CD} depends on the achiral and chiral molecular susceptibilities of the fibers, the phase differences between the susceptibilities, Δ, as well as the out-of-plane tilt angle of the fiber, α. When chiral susceptibilities and phase differences are small, the CA_{CD} can be attributed mainly to the achiral properties of the sample, therefore allowing to extract the *R*-ratio.

We have previously shown that the achiral molecular $\chi^{(2)}$ tensor components are in phase with each other, and therefore, $\Delta_{zzz,xxz} = \Delta_{zxx,xxz} = 0$ can be assumed [30]. Furthermore, it is shown that $\chi^{(2)}_{xxz}/\chi^{(2)}_{zxx} = 1$ to a good approximation [37, 50]. By assuming these conditions, CA_{CD} can be simplified to:

$$CA_{CD} = \frac{4R + 8C^2 - 4}{R^2 - 2R + 8C^2 + 5}, \tag{8}$$

where

$$R = \frac{\chi^{(2)'}_{zzz}}{\chi^{(2)'}_{zxx}} = \frac{\chi^{(2)}_{zzz}}{\chi^{(2)}_{zxx}}\cos^2\alpha + 3\sin^2\alpha, \tag{9a}$$

$$C = \frac{\chi^{(2)'}_{xyz}}{\chi^{(2)'}_{zxx}} = \frac{\chi^{(2)}_{xyz}}{\chi^{(2)}_{zxx}} \sin\alpha. \tag{9b}$$

For samples that are in-plane (ie, $\alpha \sim 0$) or have a relatively small chiral tensor component, it can be shown that the chiral term C can be neglected, hence, the R-ratio becomes a simple function of CA_{CD}:

$$R = 1 + \frac{2}{CA_{CD}} \pm 2\sqrt{\frac{1}{(CA_{CD})^2} - 1} \tag{10}$$

Equation (8) is plotted in Figure 1 as a function of $\chi^{(2)}_{zzz}/\chi^{(2)}_{zxx}$ for different values of $\chi^{(2)}_{xyz}/\chi^{(2)}_{zxx}$, where α is fixed to be 10°. It can be seen that for $\chi^{(2)}_{xyz}/\chi^{(2)}_{zxx} < 0.2$, the CA_{CD} remains similar to the $\chi^{(2)}_{xyz}/\chi^{(2)}_{zxx} = 0$ case. For muscle with $R = 0.5$, a value of $C = 0.2R$ would result in a decrease in CA_{CD} and consequently in less than 7% overestimation of the R-ratio in Equation (10). Therefore, Equation (10) can even be applied when C-ratio is nonzero but small. In addition, due to the squared R-ratio terms in Equation (8), for a specific CA_{CD} value, two R-values exist. This is presented in Equation (10) by the plus and minus signs before the square root. If $0 < R < 3$, the plus sign is to be taken for the $CA_{CD} > 0$ values and the minus sign for $CA_{CD} < 0$. Further, Equation (8) is plotted in Figure 2 as a function of α for different values of $\chi^{(2)}_{xyz}/\chi^{(2)}_{zxx}$. It can be seen that the CA_{CD} is an even function with respect to α and for small angles, all $\chi^{(2)}_{xyz}/\chi^{(2)}_{zxx}$ values result in a similar value for CA_{CD}.

From Equation (2), it can be seen that four SHG intensity measurements are needed to determine the CA_{CD} values—outgoing I_R and I_L SHG intensity excited with incident RCP and LCP beams, respectively. Since the required outgoing SHG states are orthogonal, they can be detected in parallel. Thus, the R-ratio can be determined rapidly in a dual-shot measurement with incoming RCP and LCP states in a quick succession.

In addition, a dual-shot measurement involving both RCP and LCP input states can be used to measure the second-harmonic generation circular dichroism (SHG-CD), which is defined as the normalized difference in outgoing intensity of SHG when the sample is excited with RCP and LCP light, $(I_{RCP} - I_{LCP})/([I_{RCP} + I_{LCP}]/2)$. SHG-CD can be used to determine the presence of chirality and complex-valued $\chi^{(2)}$ tensor contributions as well as a nonzero out-of-plane orientation angle α [30]. Similar to CA_{CD}, the SHG-CD measurement can be described in terms of the measured SHG Stokes vector parameters, which in turn can be expressed in terms of Mueller matrix elements [30]:

$$\text{SHG-CD} = 2\frac{s'_{0,5} - s'_{0,6}}{s'_{0,5} + s'_{0,6}} = 4\frac{\mathcal{M}_{0,8} - \mathcal{M}_{0,9}}{\sqrt{6}\mathcal{M}_{0,1} - \sqrt{3}\mathcal{M}_{0,2} - \mathcal{M}_{0,4}}. \tag{11}$$

It can be then written in terms of the products of the magnitudes of the molecular susceptibility tensor

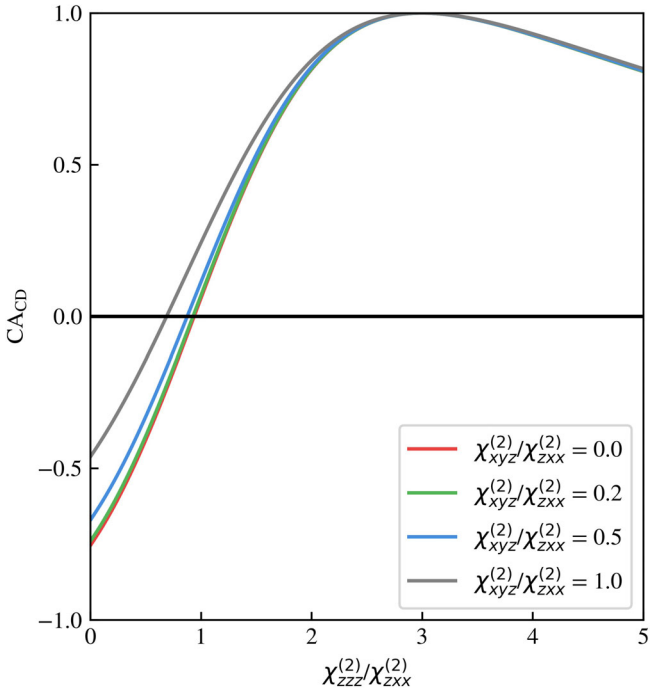

FIGURE 1 CA_{CD} as a function of $\chi^{(2)}_{zzz}/\chi^{(2)}_{zxx}$ for different values of $\chi^{(2)}_{xyz}/\chi^{(2)}_{zxx}$. The angle α is assumed to be 10°

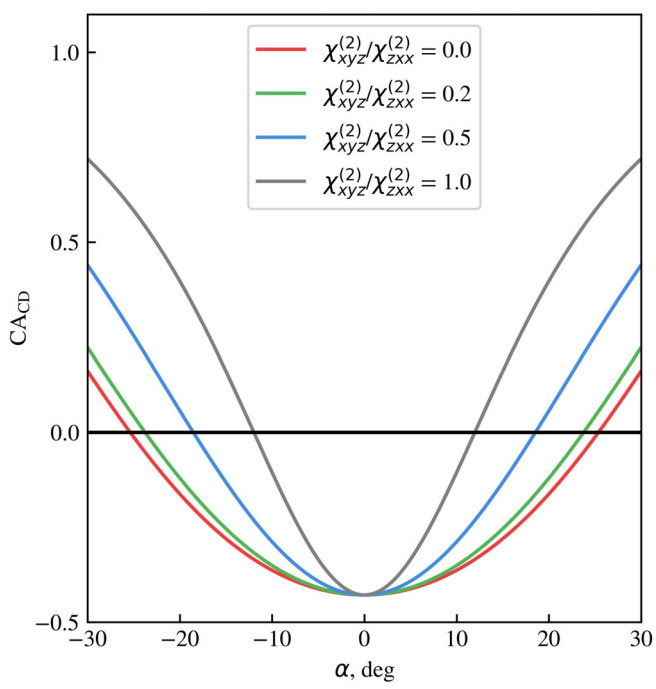

FIGURE 2 CA_{CD} as a function of α for different values of $\chi^{(2)}_{xyz}/\chi^{(2)}_{zxx}$. The $\chi^{(2)}_{zzz}/\chi^{(2)}_{zxx}$ is assumed to be 0.55

elements, the associated molecular phase differences, and the out-of-plane tilt angle of the fibers:

$$\begin{aligned}\text{SHG-CD}_{\text{numerator}} &= 2\left|\chi^{(2)}_{xyz}\right|\sin(2\alpha)\cos^3(\alpha)\\ &[\left|\chi^{(2)}_{zzz}\right|\sin\Delta_{zzz,xyz} - \left|\chi^{(2)}_{zxx}\right|\sin\Delta_{zxx,xyz}\\ &-2\left|\chi^{(2)}_{xxz}\right|\sin\Delta_{xxz,xyz}].\end{aligned} \tag{12}$$

The denominator of SHG-CD is the same as the denominator for CA_{CD} in Equation (7).

Interestingly, for achiral samples (which can be described by the C_{6v} symmetry class), that have a real-valued $\chi^{(2)}$ with $\chi^{(2)}_{xxz}/\chi^{(2)}_{zxx} = 1$, the s_0 components become the same for RCP and LCP incident polarizations and the s_3 components become equal in magnitude and opposite in sign. As a result, the circular anisotropy and thus the *R*-ratio can be estimated from a single-shot experiment using the incident light with either right- or left-hand circular polarizations (CA_R or CA_L, respectively), enabling high-throughput *R*-ratio measurement. In addition, the SHG-CD can be used to validate the small *C*-ratio approximation and if the single-shot measurement can be used to a good approximation to extract the *R*-ratio.

3 | MATERIALS AND METHODS

3.1 | Experimental setup

To demonstrate dual- and single-shot measurements of the *R*-ratio, a custom SHG microscope was coupled to an in-house built diode-pumped Yb-ion-doped potassium gadolinium tungstate (Yb:KGW) crystal-based oscillator [51] operating at a 1028 nm wavelength and generating 430 fs pulses at a 14.3 MHz repetition rate. The microscope, as described in details elsewhere [27], contains a polarization state generator (PSG) before the excitation objective (20 ×, 0.75 NA, Zeiss) and a polarization state analyzer (PSA) located between a custom 0.85 NA collection objective and the detector. The PSG contains a linear polarizer (Thorlabs LPNIR100), a half-wave plate (HWP) and a quarter-wave plate (QWP). The PSA contains a HWP, a QWP (all wave plates are from Eksma Optics, 461-4208, 461-4408, 461-4232, 461-4432, respectively) and a linear polarizer (Thorlabs LPVISA100). The PSG was set sequentially to nine different polarization states and for each polarization state the Stokes parameters of the SHG signal were measured using the PSA. For dual-shot technique, both incoming and outgoing RCP and LCP are used, while for the single-shot experiment only one of the incident polarizations (RCP, or LCP) is used, while recording both RCP and LCP polarization SHG images. The sample was raster-scanned using a resonant (EOPC SC30) and galvanometric (Cambridge Technology 6220H) mirror pair. A BG 39 filter and a 510-520 nm band-pass interference filter (Edmund Optics) were used to separate the SHG with 514 nm central wavelength from the incident light. The SHG signal was collected using a photon-counting photomultiplier module (Hamamatsu H7422P-40). Photon counts were fed into a high-throughput FPGA-based data acquisition card (Innovative Integration X5-210M) running a custom firmware. The recorded data was processed by a combination of custom software written in LabVIEW (National Instruments), MATLAB (Mathworks), and C++, which implements DSMP analysis and visualization. The full width at half maximum of the axial point spread function for the microscope with 0.75 NA objective was 1 μm radially and 3.7 μm axially.

3.2 | Sample preparation

Muscle samples were prepared from *Drosophila melanogaster* third instar larvae. The larva was submerged dorsal side up in zero calcium hemolymph-like 3 (HL3) solution [52] and dissected along the dorsal midline. After removing the internal organs, the body was unfurled to expose the body wall muscles. The sample was then fixed in 4% formaldehyde in HL3 for 20 min. After several washes in fresh buffer, the sample was sandwiched between a 1 mm-thick microscope slide and a 0.2 mm-thick coverslip without a spacer and sealed with nail polish. The sample is estimated to be 100 μm thick.

4 | RESULTS AND DISCUSSION

To validate the dual- and single-shot *R*-ratio measurement techniques, DSMP measurements were performed on the muscle sample and the *R* and *C*-ratios were obtained. Then, using s_0 and s_3 SHG images for RCP and LCP inputs extracted from the DSMP dataset, SHG-CD [30] and CA_{CD} values were calculated. CA-values were also calculated separately for right- and left-circularly polarized incident beam (CA_R or CA_L, respectively). The CA_{CD} was used for the dual-shot *R*-ratio measurement while the CA (either CA_R or CA_L) values were used for single-shot *R*-ratio measurement. The *R*-ratios obtained from full DSMP, the dual-shot technique and the single-shot technique were compared.

The combined intensity of the 36 images of a full DSMP measurement of the muscle sample is shown in Figure 3A. A characteristic striated muscle sarcomere structure with clearly resolved anisotropic bands and M-lines can be observed [7, 53]. The muscle fibers are

aligned with the Z-axis of the laboratory frame of reference, which is horizontal in the image. The SHG-CD and CA_{CD} values extracted from the DSMP dataset are presented in Figure 3B,C, respectively. The SHG-CD histogram shows a normal distribution with a mean 0.02 and a standard deviation of 0.16 indicating that most fibers are in the image plane ($\alpha = 0$) [30]. Therefore, the sample structure can be described by a C_{6v} model [30]. The CA_{CD} has a clear negative bias with its histogram being centered around −0.44 with a standard deviation of 0.16, which is consistent with a C_{6v} symmetry case and the R-ratio of ≈ 0.5 according to Equation (10) (see also Figure 1).

Having the fibers oriented in the image plane ($\alpha = 0$), the per-pixel R-ratio was determined by fitting a C_{6v} tensor model to the DSMP dataset, and the obtained values are represented as a color-coded map in Figure 4A. The R-ratio histograms are plotted over the color bar below each panel. The average value of the DSMP R-ratio is 0.53 and the standard deviation is 0.14. This is a typical range for R-ratio values in muscle fibers [26, 27, 48]. The dual-shot R-ratio is calculated from the CA_{CD} values (Figure 3) using Equation (10) and presented in Figure 4B. The obtained R-ratio distribution is centered at 0.54 with a standard deviation of 0.15. The ratio map has somewhat lower SNR compared to the full DSMP measurement, and the histogram has a wider spread accordingly, which is reasonable considering that fewer images and thus less SHG signal was used.

Since the SHG-CD is close to 0, it can be assumed that the chiral contribution is zero and the $\chi^{(2)}$ elements are real-valued. In addition, it has been previously shown that $\chi^{(2)}_{xxz}/\chi^{(2)}_{zxx} = 1$ for muscle [27]. The R-ratio can therefore be estimated in a single-shot measurement using any one of the incident circular polarizations. Figure 4C,D shows the R-ratio maps for incident RCP and LCP states, respectively. The single-shot R-ratio with RCP shows a normal distribution with a mean value of 0.54 and a standard deviation of 0.21, while the single-shot R-ratio with LCP shows a normal distribution around 0.52 with a standard deviation of 0.21. As it can be seen, the R-ratio values obtained using full DSMP, dual-shot, and single-shot measurement techniques are very similar and no statistically significant differences were observed. Therefore, the presented fast polarimetry techniques can be used for fast R-ratio measurement of muscle structures. It should be noted that, the in-plane orientation-independent extraction of the R-ratio also allows to obtain the ratio images when muscle fibrils change orientation, for example during muscle contraction. Further, these techniques can be used for large-area polarimetric tissue imaging where high imaging throughput is essential.

5 | CONCLUSION

The results presented in this work show that P-SHG microscopy can be used to characterize the molecular

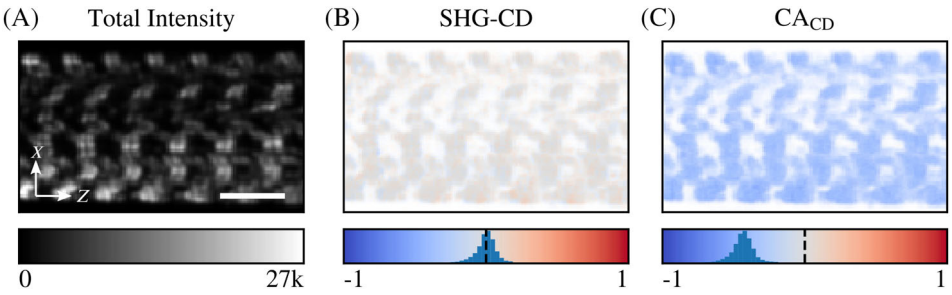

FIGURE 3 SHG microscopy images of body wall muscle fibers from a *Drosophila* third instar larva. A, Total SHG intensity of the 36 images obtained in a full DSMP experiment, B, SHG-CD of the sample, C, CA_{CD} of the sample. The scale bar is 10 μm

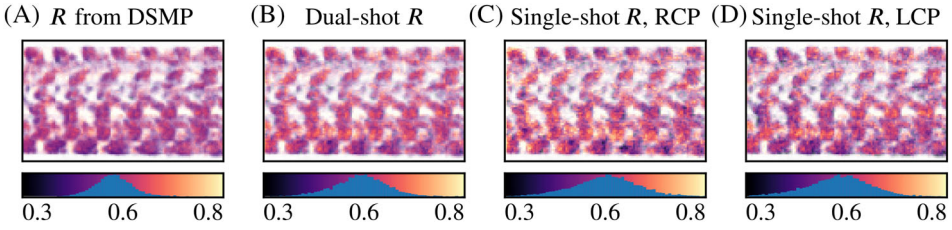

FIGURE 4 *R*-ratio maps obtained from the same muscle structure using different polarimetry methods. A, *R*-ratio extracted using all 36 DSMP dataset by fitting a C_{6v} model. B, Dual-shot *R*-ratio extracted from the CA_{CD} parameter. C, Single-shot *R*-ratio extracted from CA_R. D, Single-shot *R*-ratio extracted from CA_L. The histograms below each panel show the extracted *R*-ratio distributions, which are very similar

structure of non-centrosymmetric biological samples such as muscle using circularly polarized excitation light and circularly polarized SHG detection. The presented fast polarimetry techniques can measure the $R=\chi^{(2)'}_{zzz}/\chi^{(2)'}_{zxx}$ for samples possessing real-valued C_{6v} symmetry in a dual- or even a single-shot measurement, where there is no data fitting required. The measurement of the *R*-ratio is independent of the in-plane orientation of the sample. The instantaneous *R*-ratio estimation makes this technique applicable for imaging live samples that show fast structural dynamics and also for high-throughput whole slide imaging where the sample exposure time and acquisition time are limiting factors. These techniques can be integrated with both laser scanning and wide-field SHG microscopes.

ACKNOWLEDGMENTS

This work was supported by Natural Sciences and Engineering Research Council of Canada (NSERC) (RGPIN-2017-06923, DGDND-2017-00099, CHRPJ 462842-14), the Canadian Institutes of Health Research (CIHR) (CPG-134752), and European Regional Development Fund (project No 01.2.2.-LMT-K-718-02-0016) under grant agreement with the Research Council of Lithuania (LMTLT).

ORCID

Ahmad Golaraei https://orcid.org/0000-0001-8885-2360

REFERENCES

[1] A. Erikson, J. Örtegren, T. Hompland, C. de Lange Davies, M. Lindgren, *J. Biomed. Opt.* **2007**, *12*(4), 044002.
[2] I. Freund, M. Deutsch, *Opt. Lett.* **1986**, *11*(2), 94.
[3] S. Roth, I. Freund, *J. Chem. Phys.* **1979**, *70*(4), 1637.
[4] S. Roth, I. Freund, *Biopolymers* **1981**, *20*(6), 1271.
[5] S.-W. Chu, S.-Y. Chen, G.-W. Chern, T.-H. Tsai, Y.-C. Chen, B.-L. Lin, C.-K. Sun, *Biophys. J.* **2004**, *86*(6), 3914.
[6] F. Tiaho, G. Recher, D. Rouède, *Opt. Express* **2007**, *15*(19), 12286.
[7] V. Barzda, C. Greenhalgh, J. Aus der Au, S. Elmore, J. van Beek, J. Squier, *Opt. Express* **2005**, *13*(20), 8263.
[8] S. V. Plotnikov, A. C. Millard, P. J. Campagnola, W. Mohler, *Biophys. J.* **2006**, *90*(2), 693.
[9] V. Nucciotti, C. Stringari, L. Sacconi, F. Vanzi, L. Fusi, M. Linari, G. Piazzesi, V. Lombardi, F. S. Pavone, *Proc. Natl. A Sci.* **2010**, *107*(17), 7763.
[10] S. Psilodimitrakopoulos, P. Loza-Alvarez, D. Artigas, *Biomed. Opt. Express* **2014**, *5*(12), 4362.
[11] D. A. Dombeck, K. A. Kasischke, H. D. Vishwasrao, M. Ingelsson, B. T. Hyman, W. W. Webb, *Proc. Natl. A Sci.* **2003**, *100*(12), 7081.
[12] C. H. Yu, N. Langowitz, H. Y. Wu, R. Farhadifar, J. Brugues, T. Y. Yoo, D. Needleman, *Biophys. J.* **2014**, *106*(8), 1578.
[13] G. Mizutani, Y. Sonoda, H. Sano, M. Sakamoto, T. Takahashi, S. Ushioda, *J. Lumin.* **2000**, *87*, 824.
[14] N. Mazumder, L. Yun Xiang, J. Qiu, F. J. Kao, *Sci. Rep. UK* **2017**, *7*(April), 1.
[15] R. Cisek, D. Tokarz, S. Krouglov, M. Steup, M. J. Emes, I. J. Tetlow, V. Barzda, *J. Phys. Chem. B* **2014**, *118*(51), 14785.
[16] R. Cisek, D. Tokarz, L. Kontenis, V. Barzda, M. Steup, *Starch/Staerke* **2017**, *1700031*, 1.
[17] I. Freund, M. Deutsch, A. Sprecher, *Biophys. J.* **1986**, *50*(4), 693.
[18] P. Stoller, B. M. Kim, A. M. Rubenchik, K. M. Reiser, L. B. Da Silva, *J. Biomed. Opt.* **2002**, *7*(2), 205.
[19] P. Stoller, P. M. Celliers, K. M. Reiser, A. M. Rubenchik, *Appl. Opt.* **2003**, *42*(25), 5209.
[20] J. Duboisset, D. Aït-Belkacem, M. Roche, H. Rigneault, S. Brasselet, *Phys. Rev. A* **2012**, *85*(4), 1.
[21] I. Gusachenko, G. Latour, M. C. Schanne-Klein, *Opt. Express* **2010**, *18*(18), 19339.
[22] I. Gusachenko, V. Tran, Y. G. Houssen, J. M. Allain, M. C. Schanne-Klein, *Biophys. J.* **2012**, *102*(9), 2220.
[23] O. Nadiarnykh, P.l. J. Campagnola, *Opt. Express* **2009**, *17*(7), 5794.
[24] P. J. Su, W. L. Chen, T. H. Li, C. K. Chou, T. H. Chen, Y. Y. Ho, C. H. Huang, S. J. Chang, Y. Y. Huang, H. S. Lee, C. Y. Dong, *Biomaterials* **2010**, *31*(36), 9415.
[25] A. E. Tuer, S. Krouglov, N. Prent, R. Cisek, D. Sandkuijl, K. Yasufuku, B. C. Wilson, V. Barzda, *J. Phys. Chem. B* **2011**, *115*(44), 12759.
[26] M. Samim, S. Krouglov, V. Barzda, *J. Opt. Soc. Am. B* **2015**, *32*(3), 451.
[27] L. Kontenis, M. Samim, A. Karunendiran, S. Krouglov, B. Stewart, V. Barzda, *Biomed. Opt. Express* **2016**, *7*(2), 559.
[28] P. J. Su, W. L. Chen, Y. F. Chen, C. Y. Dong, *Biophys. J.* **2011**, *100*(8), 2053.
[29] A. Golaraei, K. Mirsanaye, Y. Ro, S. Krouglov, M. K. Akens, B. C. Wilson, V. Barzda, *J. Biophotonics* **2018**, *2018*, 1.
[30] A. Golaraei, K. Kontenis, K. Mirsanaye, S. Krouglov, M. K. Akens, B. C. Wilson, V. Barzda, *Sci. Rep. UK* **2019**, *9*(1), 1.
[31] A. E. Tuer, M. K. Akens, S. Krouglov, D. Sandkuijl, B. C. Wilson, C. M. Whyne, V. Barzda, *Biophys. J.* **2012**, *103*(10), 2093.
[32] M. Burke, A. Golaraei, A. Atkins, M. Akens, V. Barzda, C. Whyne, *J. Struct. Biol.* **2017**, *199*(2), 153.
[33] S. Schürmann, F. Von Wegner, R. H. A. Fink, O. Friedrich, M. Vogel, *Biophys. J.* **2010**, *99*(6), 1842.
[34] M. Dubreuil, F. Tissier, L. Le Roy, J.-P. Pennec, S. Rivet, M.-A. Giroux-Metges, Y. Le Grand, *Biomed. Opt. Express* **2018**, *9*(12), 6350.
[35] C. Yuan, Z. Wang, T. K. Borg, T. Ye, C. Baicu, A. Bradshaw, M. Zile, R. B. Runyan, Y. Shao, B. Z. Gao, *Biomed. Opt. Express* **2019**, *10*(7), 3183.
[36] A. Golaraei, R. Cisek, S. Krouglov, R. Navab, C. Niu, S. Sakashita, K. Yasufuku, M. S. Tsao, B. C. Wilson, V. Barzda, *Biomed. Opt. Express* **2014**, *5*, 3562.
[37] A. Golaraei, L. Kontenis, R. Cisek, D. Tokarz, S. J. Done, B. C. Wilson, V. Barzda, *Biomed. Opt. Express* **2016**, *7*(10), 4054.
[38] D. Tokarz, R. Cisek, A. Golaraei, S. L. Asa, V. Barzda, B. C. Wilson, *Biomed. Opt. Express* **2015**, *6*(9), 3475.
[39] D. Tokarz, R. Cisek, A. Joseph, A. Golaraei, K. Mirsanaye, S. Krouglov, S. L. Asa, B. C. Wilson, V. Barzda, *Front. Oncol.* **2019**, *9*(MAR), 1.

[40] C.-H. Lien, K. Tilbury, S.-J. Chen, P. J. Campagnola, *Opt. Express* **2013**, *4*(10), 1991.
[41] E. L. Dewalt, S. Z. Sullivan, P. D. Schmitt, R. D. Muir, G. J. Simpson, *Anal. Chem.* **2014**, *86*(16), 8448.
[42] Y. Tanaka, E. Hase, S. Fukushima, Y. Ogura, T. Yamashita, T. Hirao, T. Araki, T. Yasui, *Biomed. Opt. Express* **2014**, *5*(4), 1099.
[43] G. Ducourthial, J. S. Affagard, M. Schmeltz, X. Solinas, M. Lopez-Poncelas, C. Bonod-Bidaud, R. Rubio-Amador, F. Ruggiero, J. M. Allain, E. Beaurepaire, M. C. Schanne-Klein, *J. Biophotonics* **2018**, *2019*, 1.
[44] R. Carriles, K. E. Sheetz, E. E. Hoover, J. A. Squier, V. Barzda, *Opt. Express* **2008**, *16*(14), 10364.
[45] D. Sandkuijl, R. Cisek, A. Major, V. Barzda, *Biomed. Opt. Express* **2010**, *1*(3), 895.
[46] N. Mazumder, J. Qiu, M. R. Foreman, C. M. Romero, C.-W. Hu, H.-R. Tsai, P. Török, F.-J. Kao, *Opt. Express* **2012**, *20* (13), 14090.
[47] M. Förderer, T. Georgiev, M. Mosqueira, R. H. A. Fink, M. Vogel, *Biomed. Opt. Express* **2016**, *7*(2), 525.
[48] C. Odin, T. Guilbert, A. Alkilani, O. P. Boryskina, V. Fleury, Y. Le Grand, *Opt. Express* **2008**, *16*(20), 16151.
[49] H. Zhao, R. Cisek, A. Karunendiran, B. A. Tokarz, V. B. Stewart, *Biomed. Opt. Express* **2019**, *10*(10), 5130.
[50] C. A. Dailey, B. J. Burke, G. J. Simpson, *Chem. Phys. Lett.* **2004**, *390*(1), 8.
[51] A. Major, R. Cisek, V. Barzda, *Opt. Express* **2006**, *14*(25), 12163.
[52] B. A. Stewart, H. L. Atwood, J. J. Renger, J. Wang, C. F. Wu, *J. Comp. Physiol. A* **1994**, *175*(2), 179.
[53] P. J. Campagnola, A. C. Millard, M. Terasaki, P. E. Hoppe, C. J. Malone, W. A. Mohler, *Biophys. J.* **2002**, *82*(1), 493.

How to cite this article: Golaraei A, Kontenis L, Karunendiran A, Stewart BA, Barzda V. Dual- and single-shot susceptibility ratio measurements with circular polarizations in second-harmonic generation microscopy. *J. Biophotonics*. 2020; e201960167. https://doi.org/10.1002/jbio.201960167